IEEE Access
Multidisciplinary ⋮ Rapid Review ⋮ Open Access Journal

Received April 5, 2022, accepted May 1, 2022, date of publication May 11, 2022, date of current version May 16, 2022.

Digital Object Identifier 10.1109/ACCESS.2022.3174227

A GaN Microwave Power Amplifier Design Based on the Source/Load Pull Impedance Modeling via Virtual Gain Optimization

SEDAT KILINC[1,2], BINBOGA SIDDIK YARMAN[1,2,3,4], (Life Fellow, IEEE), AND SERDAR OZOGUZ[2]

[1]Department of Electrical-Electronics Engineering, Istanbul University-Cerrahpaşa, 34320 Istanbul, Turkey
[2]Department of Electronics and Communication Engineering, Istanbul Technical University, 34469 Istanbul, Turkey
[3]RFT Research Corporation of Teknopark, 34906 Istanbul, Turkey
[4]Savronik Electronics Corporation, 34744 Istanbul, Turkey

Corresponding author: Binboga Siddik Yarman (sbyarman@gmail.com)

This work was sponsored by Savronik Elektronik Corporation of Turkey.

ABSTRACT Generation of proper source/load pull impedances for a selected GaN device is essential to design a microwave power amplifier for optimum gain and power-added efficiency. As they are obtained, these impedances may not be realizable network functions over the desired frequency band. Therefore, in this paper, first, we introduce a new method to test if the given source and load pull impedances are realizable. Then, a novel numerical procedure is introduced to model the source and load pull impedances as realizable network functions, which in turn results in the optimum power intake and power delivering capacity for the GaN transistor used in the design. In the numerical modelling process, a robust tool called ''Virtual Gain Optimization'' is presented. Numerically generated realizable source and load impedances are modelled analytically. Eventually, these impedances are synthesized using our automatic Darlington Synthesis Robot software to yield the optimum input and output matching network topologies with component values. Examples are presented to test the realizability of the given source/load pull impedance data. Then, the power intake and delivery capacity of the active device are assessed for a 10W-GaN power transistor, namely ''Wolfspeed CGH40010F'' over 0.8-3.0 GHz bandwidth. Eventually, the power amplifier is designed and manufactured. It is shown that the computed and the measured performance of the amplifier is very close with 10 Watts output power, 11.4 ± 0.6 dB gain and 49% to 76 % power added efficiency.

INDEX TERMS Broadband matching, broadband power amplifiers, assessment of the nonlinear behavior of an active device, realizability quest of the optimum source/load pull impedances, real frequency techniques, power intake/delivery performance of a GaN transistor.

I. INTRODUCTION

For wireless communication systems, it is essential to design power amplifiers (PA) for a variety of applications [1]–[9]. Nowadays, it is a common practice to employ Gallium Nitrate (*GaN*) transistors due to their high-power delivery capacity [10]–[13]. In practice, PA design process starts with careful selection of the power transistor considering the design parameters such as the required output signal power to be delivered, power added efficiency (PAE) of the amplifier, transducer power gain (TPG) over the specified bandwidth and etc. Once the power transistor is selected, its nonlinear behavior is characterized by determining the optimum source-pull (SP) and load-pull (LP) impedances. This process is achieved at each frequency by terminating the device with various impedance values, measuring the pre-set performance criteria such as gain, efficiency and harmonics. In this regard, the real and the imaginary parts of the impedances are swept in a particular impedance zone on the Smith Chart to determine the optimum source and load impedances. In practice, optimum source and load impedances are published by the nonlinear active device manufacturers as in [14]. Based on the published data, one can easily make a narrow bandwidth PA design, per say, at a single frequency f_a on the measured source and load pull impedance data. However, the design task becomes difficult if

The associate editor coordinating the review of this manuscript and approving it for publication was Chao-Yang Chen.

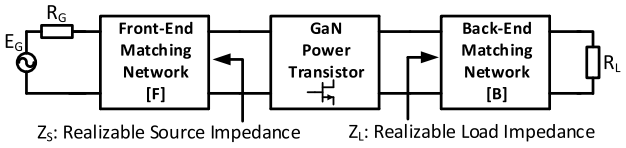

FIGURE 1. A typical microwave power amplifier with realizable source and load impedances Z_S and Z_L.

the bandwidth increases. For broadband PA design, we need to determine source and load pull impedance data at a sufficiently large number of discrete frequencies to optimize the PA performance inside the frequency band of interest. In this case, resulting source and load pull impedance data sets must correspond to realizable network functions, which eventually, yield optimum input and output matching networks, when they are modelled as positive real functions [15]–[18].

Let $Z_{SPa}(j\omega_a) = R_{SPa}(\omega_a) + jX_{SPa}(\omega_a)$ and $Z_{LPa}(j\omega_a) = R_{LPa}(\omega_a) + jX_{LPa}(\omega_a)$ designate the discrete actual source and load pull impedance data at the actual angular frequency $\omega_a = 2\pi f_a$ with actual frequency f_a. In these notations, subscript "a" refers to measured actual values. To simplify the PA design process, measured impedance data is normalized with respect to a normalization resistance R_0 and a frequency f_{0a}. In practice, R_0 may be selected as the standard termination 50Ω and f_{0a} can be chosen at the high end of the frequency band. In this case, normalized angular frequencies are mapped by the formula $\omega = \frac{2\pi f_a}{2\pi f_{a0}} = \frac{\omega_a}{\omega_{a0}} = \frac{f_a}{f_{0a}}$, which defines the normalized angular frequencies $\omega = 2\pi f$. It is noted that, in this representation, high end of the frequency band corresponds to normalized angular frequency ω_{he} such that $\omega_{he} = 1$. In other words, normalized high-end frequency of the passband is given by $f = f_{he} = \frac{1}{2\pi}$, Using the generic notation, a normalized impedance $Z(j\omega)$ is obtained by dividing the actual impedance $Z_a(j\omega_a) = R_a(\omega_a) + jX_a(\omega_a)$ to R_0 such that $Z(j\omega) = \frac{Z_a}{R_0} = R(\omega) + jX(\omega)$. Likewise, normalized SP and LP impedances are represented by $Z_{SP}(j\omega) = R_{SP}(\omega) + jX_{SP}(\omega)$ and $Z_{LP}(j\omega) = R_{LP}(\omega) + jX_{LP}(\omega)$ respectively. Note that the measured SP and LP terminations may optimize the *TPG*, *PAE* and the harmonics of the amplifier under consideration. Obviously, source and load pull impedances must be positive real (PR) functions so that one is able to analytically model the measured data and construct the front and the back-end matching networks as depicted in Fig. 1.

As they are placed on the Smith Chart, discrete source and load pull impedances may not describe positive real functions over broad frequency band. For the actual realization of the input and the output matching networks of the PA, it may be useful to develop a test procedure to determine if Z_{SP} and Z_{LP} are PR functions. Eventually, the best possible-realizable source and load impedances must be generated to yield the front and the back-end matching networks for the power amplifier to be designed. Therefore, in the following section, we introduce a novel numerical method to test the positive realness of a given discrete impedance data (Section II). Then, examples are given to test if a measured arbitrary immittance data and the source/load pull impedances obtained from the Wolfspeed's CGH40010F *GaN* power transistor, represent positive real functions (Section III). In section IV, we propose a novel numerical procedure to assess the power intake and power delivery capacity of given immittance data. In section V and in Section VI, we specifically investigated the power intake/power delivery performance of the source and the load pull impedance data belongs to CGH40010F over 0.8-3GHz using the "Real Frequency-Line Segment Technique (RF-LST)" [19]–[22]. During the numerical performance assessments process, we introduce an original tool called "Virtual Gain Optimization (VGO)". In Section VII, we introduce a new method to generate an analytic model for the given realizable immittance data. For the sake of completeness, in Section VIII, the parametric method to build analytic positive real functions is summarized. In Section IX, the proposed analytic model technique is employed to build the rational impedance forms for the optimum source and load pull data obtained via RF-LST. In Section X, the designed and constructed power amplifier is presented. Finally, the paper is concluded in Section XI.

II. A NUMERICAL APPROACH TO TEST THE POSITIVE REALNESS OF THE MEASURED SP AND LP IMMITTANCE DATA

While playing with an immittance data on the Smith Chart, microwave engineers may not know if the data placed on the Smith Chart with positive real part represent a realizable passive immittance function. From the matching theory point of view, this fact unexpectedly penalizes the performance of the matched system under consideration. Therefore, one needs to test the data whether it is a real-realizable immittance or not over the useful frequency bands. This test is extremely useful to assess the quality of match for the given impedance. In this regard, let us briefly review some major properties of realizable immittance functions.

Any complex analytic function $K(p)$ is called positive real (PR) or realizable immittance function if and only if $K(p)$ is real when p is real (i.e. $p = \sigma$) and $K(\sigma) \geq 0$ when $\sigma \geq 0$. In this notation $p = \sigma + j\omega$ is the complex Laplace plane variable.

A positive real function $K_m(p) = \frac{a_m(p)}{b_m(p)}$ is called a minimum function if it is free of $j\omega$ poles.

A positive real function $K_F(p) = a_F(p)/b_F(p)$, is called a Foster function if $\frac{dX_F(\omega)}{d\omega} > 0$ with $K_F(j\omega) = jX_F(\omega)$.

It is crucial to emphasize that any positive real function $K(p) = \frac{a(p)}{b(p)}$ may be decomposed in to its minimum and Foster functions such that

$$K(p) = K_m(p) + K_F(p) \tag{1a}$$

where

$$K_m(p) = \frac{a_m(p)}{b_m(p)} = \sum_{i=1}^{n} \frac{k_i}{p - p_i} \tag{1b}$$

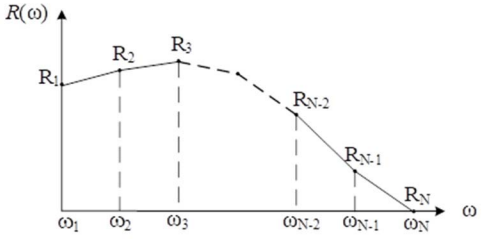

FIGURE 2. Piecewise linearization of the Real part $R(\omega)$ of a minimum function $K_m(j\omega) = R(\omega) + jX_m(\omega)$.

where $p_i = \sigma_i + j\omega_i$ and $p_{i+1} = \sigma_i - j\omega_i$ with $\sigma_i < 0$ are the strictly left half plane zeros of the denominator polynomial $b_m(p)$ of (1b).

On the $j\omega$ axis, $K_F(p)$, $K(p)$, and $K_m(p)$ are expressed as

$$K_F(j\omega) = jX_F(\omega) \tag{2a}$$
$$K(j\omega) = R(\omega) + jX(\omega) \tag{2b}$$
$$K_m(j\omega) = R(\omega) + jX_m(\omega) \tag{2c}$$

As stated above, for a Foster function $K_F(j\omega) = jX_F(\omega)$, derivative of $X_F(\omega)$ with respect to ω is always non-negative. In the case, we can introduce the following theorem to provide the necessary background to test the positive realness or equivalently realizability of an immittance function.

Theorem 1 A minimum function $K_m(j\omega)$ is uniquely determined from its real part $R(\omega)$ using Hilbert transformation such that

$$X_m(\omega) = R_\infty + \frac{2\omega}{\pi}\int_0^\infty \frac{R(y)}{y^2-\omega^2}dy = H\{R(\omega)\} \tag{3}$$

For a minimum function $K_m(j\omega)$, the relation between its real part $R(\omega)$ and its imaginary part $X(\omega)$ is called the Hilbert transformation (HT). In this paper, HT operator is designated by $H\{.\}$. Thus, we say that $X_m(\omega) = H\{R(\omega)\}$.

A. NUMERICAL EVALUATION OF HILBERT TRANSFORMATION

The real part $R(\omega)$ of a minimum function may be piece-wise linearized as shown in Fig. 2. In this figure, $R(\omega)$ is sampled at the break frequencies $\{\omega_1, \omega_2, \omega_3, \ldots \omega_N\}$ with corresponding break points $\{R_1, R_2, R_3, \ldots R_N\}$. Furthermore, it is assumed that adjacent sampled pairs $\{\omega_j, R_j\}$ and $\{\omega_{j+1}, R_{j+1}\}$ are connected by line segments. For a sufficiently large frequency placed at $\omega = \omega_N$, $R(\omega)$ becomes practically zero yielding $R_N \cong 0$. Referring to Fig.2, $R(\omega)$ is simply evaluated using (4) such that

$$R_j(\omega) = a_j\omega + b_j; \quad \omega_j \le \omega \le \omega_{j+1};\ j = 1, 2, \ldots, N \tag{4a}$$

where

$$a_j = \frac{R_j - R_{j+1}}{\omega_j - \omega_{j+1}} \tag{4b}$$

and

$$b_j = \frac{(R_{j+1})\omega_j - (R_j)\omega_{j+1}}{\omega_{j-\omega_{j+1}}} \tag{4c}$$

In the above representation of $R(\omega)$, we assume that $R_\infty = R(\omega)$ is zero. This is a practical assumption for all band limited amplifier designs such as lowpass and bandpass.

Having line-segment representation of $R(\omega)$, imaginary part $X_m(\omega)$ of (3) is derived as

$$X_m(\omega) = \sum_{j=1}^{N-1} \beta_j(\omega)\Delta R_j H\{R(\omega)\} \tag{5a}$$

where the excursion ΔR_j and the coefficients $\beta_j(\omega)$ are given by

$$\Delta R_j = R_{j+1} - R_j \tag{5b}$$
$$F_j(\omega) = (\omega + \omega_j)\ln(|\omega + \omega_j|) + (\omega - \omega_j)\ln(|\omega - \omega_j|) \tag{5c}$$
$$\beta_j(\omega) = \frac{1}{\pi(\omega_j - \omega_{j+1})}\left[F_{j+1}(\omega) - F_j(\omega)\right] \tag{5d}$$

For this work, (4) and (5) are programmed in MatLab under the functions called "*Line_Segment*" and "*Hilbert_Transform*" respectively [23]. Thus, employing the above equations, one can generate a minimum function $K_m(j\omega)$ point by point from its real part $R(\omega)$ without using any analytic forms. Resulting $K_m(j\omega) = R(\omega) + jX_m(\omega)$ is for sure positive real and realizable as a lossless two-port in Darlington sense.

In the following sub-section, we propose a novel numerical procedure to decompose a positive real function into its minimum and Foster functions.

B. NUMERICAL DECOMPOSITION OF A MEASURED IMMITTANCE DATA TO ITS MINIMUM AND FOSTER FUNCTIONS

On the real frequency axis $j\omega$, (1a) can be regarded as a Theorem as follows.

Theorem 2: Any immittance data $K(j\omega) = R(\omega) + jX(\omega)$ can be decomposed into its minimum $K_m(j\omega) = R(\omega) + jX_m(\omega)$ and Foster $K_F(j\omega) = jX_F(\omega)$ functions numerically such that

$$K(j\omega) = R(\omega) + jX(\omega) = K_m(j\omega) + K_F(j\omega) \tag{6a}$$

where

$$X_m(\omega) = H(R) \tag{6b}$$
$$X_F(\omega) = X(\omega) - X_m(\omega) \tag{6c}$$

with $\frac{dX_F(\omega)}{d\omega} \ge 0; \forall\omega$. Hence, using (6), any measured immittance data can be decomposed into its minimum and Foster functions. Then, one can test its realizability by investigating the reactance curve $X_F(\omega)$ if it is monotonically increasing. This way of analyzing the Foster Part, generates the answer for the "quest of realizability" of an immittance function.

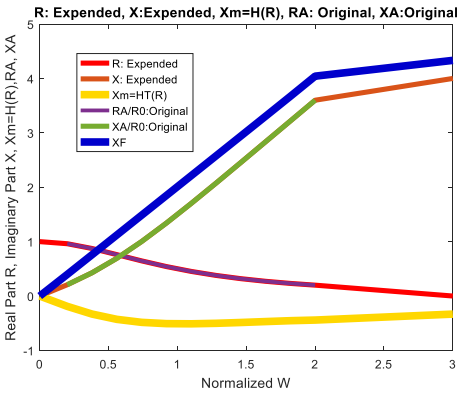

FIGURE 3. Investigation of the measured impedance data if it is a positive real function. The answer is yes. It is PR.

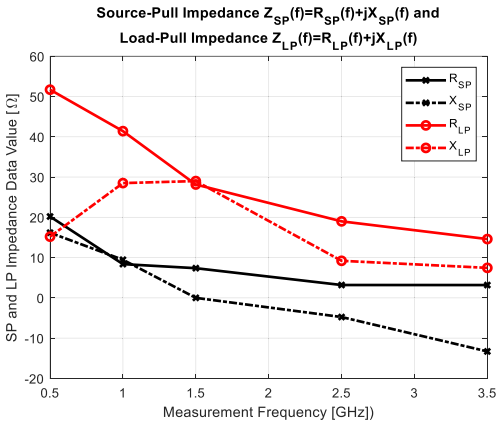

FIGURE 4. Optimum Source-Pull and Load-Pull termination impedances.

In generating $X_F(\omega)$, it is crucial to note that the measured immittance data must be extrapolated over the entire frequency band to include DC up to a frequency f_N where the real part $R(\omega_N)$ is practically zero. Likewise, the imaginary part $X(\omega)$ is also extrapolated such that $X\ (0) = 0$ and $X\ (\omega_N)$ is set to a reasonable value perhaps, by considering the immittance model, or in an ad-hoc manner to force $X_F(\omega)$ to become Foster reactance function if possible. In the following section, we present examples to test the positive realness of the given immittance data.

III. REALIZABILITY TEST EXAMPLES

A. A GENERIC TEST EXAMPLE

The measured impedance data $ZA\ (j\omega_a) = RA\ (\omega_a) + jXA(\omega_a)$ is depicted in Fig. 3 (RA : purple and XA: green plots respectively).

Measurements cover the frequency band of $f_{1a} = 0.2\,GHz$, and $f_{2a} = 2\,GHz$. Data is normalized with respect to $R_0 = 50\Omega$ and $f_0 = 1\,GHz$. Now, let us test if the measured impedance data is a positive real function.

For this purpose, we developed a MatLab program called "*Main_Check_Immittance_Data_if _PR.m*". In this program, we implemented (5) and (6) properly, plotted $X_F(\omega)$. In the computations, we used a total number of $N_S = 11$ sampling points over 200 MHz-2 GHz bandwidth. Close examination of Fig.3 reveals that, indeed $X_F(\omega)$ is monotonically increasing. Hence, $ZA\ (j\omega_a) = RA\ (\omega_a) + jXA(\omega_a)$ is a realizable data set as measured.

B. ASSESMENT OF THE REALIZIBILITY F THE SOURCE AND THE LOAD PULL IMPEDANCES OBTAINED FROM A GAN POWER TRANSISTOR

In this sub-section, we investigate the positive realness of the measured optimum source and load pull impedance data extracted from a GaN power transistor. The selected transistor is a, $CGH40010F$ from *Wolfspeed* Company with nominal 10 Watts output power [14]. As reported in [14], optimum source and load pull impedance plots are shown in Fig. 4

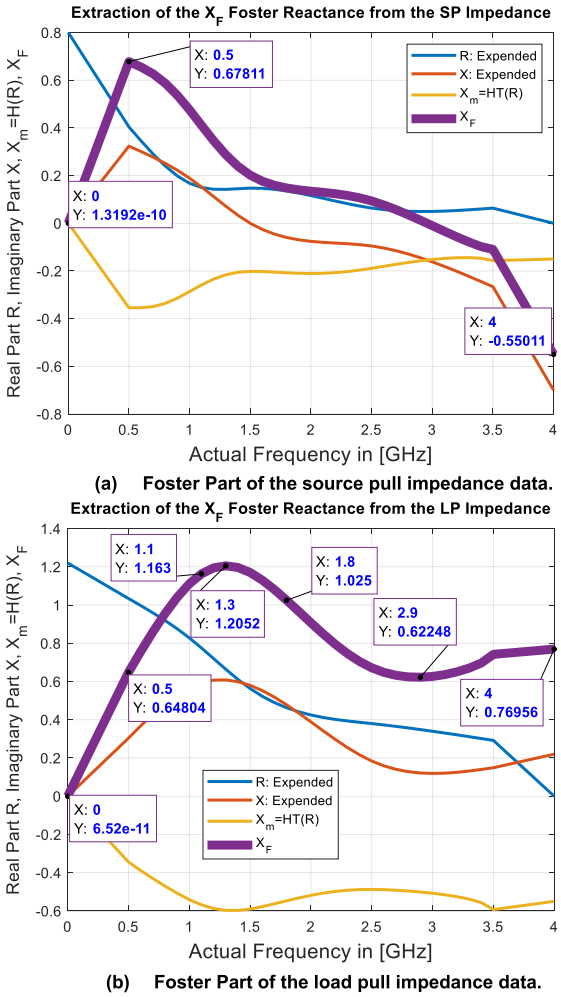

FIGURE 5. Extraction of the Foster Reactance from the source/load pull impedances.

(Black Plots: Source Pull Impedance, Red Plots: Load Pull Impedance respectively).

As described in the previous section, we extrapolated the given data to cover the frequencies $F1a = 0(DC)$ and $FNa = 4GHz$. At DC, we select $RSP(1) = 25\Omega$ and $XSP(1) = 0$.

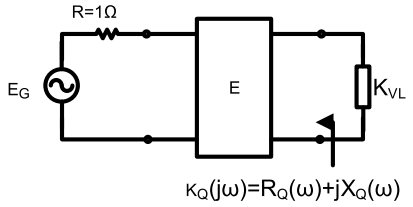

FIGURE 6. A virtual single matching problem to model a measured immittance data $K\,(j\omega)$ by setting $K_{VL} = Z^*$.

At $4GHz$, $RSP(N) = 0$ and $XSP(N) = -13.6\Omega$ are selected. Similarly, load pull impedance data is augmented as $RLP(1) = 61\Omega$, $RL(N) = 0\Omega$ and $XLP(1) = 0$, $XLP(N) = 11\Omega$.

Utilizing the proposed Algorithm, we extracted the Foster reactance functions for both Source Pull (SP) and Load Pull (LP) impedances. Results are depicted in Fig. 5.

Close examination of Fig. 5a reveals that, up to 500 MHz, the extracted Foster reactance $X_{FSP}(\omega)$ is monotonically increasing (SP: Purple Plot). Then, it drastically falls. In this case, $X_{FSP}(\omega)$ behaves like a proper Foster reactance from DC to $500MHz$. In other words, it is possible to model the given immittance data from DC to 500MHz with an analytic positive real function which yields an exact fit (Perfect Match). Then, the data is no longer Foster function. On the other hand, computed Foster portion X_{FLP} of the measured load pull impedance is good from DC up to 1.3 GHz (Band-1). Between 1.3GHz and 2.8GHz (Band-2) it decreases. Therefore, the Band-2 region is no good; indicating that, one sacrifices gain and/or power added efficiency in this band. After 2.8GHz to 4GHz (Band-3), XF_{LP} increases monotonically. Thus, we say that measured load pull impedance data behaves like a proper positive real function in Band-1 and Band-3 which leads to perfect power delivery performance.

So far, what we have observed that, due to nonlinear behavior of the GaN transistor Wolfspeed CGH40010F, reported source and load pull impedances are not realizable network functions over the frequency bands indicated above, even though they present positive real parts. However, they can be fitted to realizable network functions as much as possible, to construct the optimum front-end (input) and back-end (output) matching networks of the power amplifier by sacrificing the idealized gain and power added efficiency. This process leads us to the gain-bandwidth limitation of the active device under consideration. In the follow up section, we propose a procedure to assess the power intake/delivery performance of an active device employing the real frequency line segment technique (RF-LST).

IV. POWER INTAKE/ DELIVERY PERFORMANCE OF A REALIZABLE IMMITTANCE

The purpose of this section is to build the best realizable line-segment model for the reported source and load pulled immittances of [14] as much as possible. The proposed method is outlined as follows.

Let $K\,(j\omega) = R\,(\omega) + jX(\omega)$ refers to either the optimum source or load pull immittance to be modelled. In this regard, we define a virtual matching problem as shown in Fig. 6, where the virtual load $K_{VL}\,(j\omega) = R_{LV}\,(\omega) + jX_{VL}(\omega)$ is the complex conjugate of the immittance data to be modelled using the Real Frequency Line Segment technique [20]. In this case, the virtual load $K_{VL}\,(j\omega)$ is expressed as

$$R_{LV}\,(\omega) = R(\omega) \tag{7a}$$

$$X_{VL} = -X(\omega) \tag{7b}$$

Referring to Fig.6, in RF-LST, lossless matching network [E], is described by means of its PR driving point back-end immittance $K_Q\,(j\omega) = R_Q\,(\omega) + jX_Q(\omega)$ in Darlington sense. Furthermore, we assume that $K_Q\,(j\omega)$ is a minimum function. Therefore, $X_Q(\omega)$ is uniquely determined from $R_Q\,(\omega)$ via Hilbert Transformation as in (3). Referring to Fig. 2, the unknown of the matching problem is selected as the real part $R_Q\,(\omega)$ and it is expressed by means of its unknown break points $RQA = [R_1R_2R_3\ldots R_{N-1}R_N]$, which is sampled at the break frequencies $WBR = [\omega_1\omega_2\omega_3\ldots\omega_{N-1}\omega_N]$. $R_Q\,(\omega)$ is evaluated using (4) and $X_Q\,(\omega)$ is generated employing (5).

The unknown break points $[R_1R_2R_3\ldots R_{N-1}R_N]$ are determined to optimize the transducer power gain which is given by

$$\begin{aligned} T\,(\omega) &= \frac{Power(delivery/intake)}{Available\ Power\ of\ the\ excitation} \\ &= \frac{4R_QR_{LV}}{\left(R_Q+R_{LV}\right)^2+\left(X_Q+X_{LV}\right)^2} \\ &= \frac{4R_QR}{\left[R_Q+R\right]^2+\left[H(R_Q)-X\right]^2} \end{aligned} \tag{8}$$

During the optimization process, we target a flat gain level T_0 to minimize the error function $\varepsilon\,(\omega) = T\,(\omega) - T_0$ over the frequency band of interest. The ideal solution is the unity TPG (i.e., $T\,(\omega) = 1$) over passband, which yields $R_Q(\omega) = R(\omega)$ and $X_Q\,(\omega) = -X_{LV} = X(\omega)$ as desired. If $T(\omega)$ deviates from the unity gain, the trace of line segment model shifts from the original data. Therefore, we say that ''quality of immittance modelling'' is measured by means of the transducer power gain of the virtual matching problem over the passband. During optimization, the error function may be expressed in terms of the unknown break points as

$$\begin{aligned} \varepsilon\,(\omega) &= T(\omega)-T_0 \\ &= \frac{4R_QR}{\left[R_Q(\omega)+R(\omega)\right]^2+\left[\sum_{j=1}^{N-1}\beta_j(\omega)\Delta R_j-X(\omega)\right]^2}-T_0 \end{aligned} \tag{9a}$$

or equivalently,

$$\begin{aligned} \varepsilon\,(\omega) = 4R_QR - T_0\Bigg\{&\left[R_Q(\omega)+R(\omega)\right]^2 \\ &+\left[\sum_{j=1}^{N-1}\beta_j(\omega)\Delta R_j)-X(\omega)\right]^2\Bigg\} \end{aligned} \tag{9b}$$

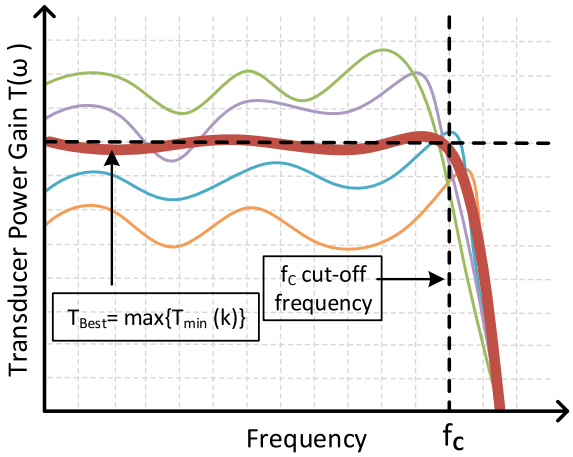

FIGURE 7. Selection of the best GBWL by sweeping $T0\,(k)$.

In (9), $R(\omega)$ and $X(\omega)$ are the augmented immittance data to be modelled. $R_Q(\omega)$ is a line between the endpoints (ω_j, R_j) and (ω_{j+1}, R_{j+1}) for $\omega \in [\omega_j, \omega_{j+1}]$ as in (4).

It must be noted that $\varepsilon\,(\omega)$ is a quadratic/convex function in the unknown break points R_j. Therefore, the numerical minimization process is always convergent, and it is possible to hit global minimum of ε yielding the **"best solution for the break points with the highest value of the minimum of the passband gain" is** $T_{Best} = max\,\{T_{min}(k)\}$ as shown in Fig.7. Based on the last statement, the following sub-section is presented to assess the numerical power delivery/intake performance of the given immittance data.

A. THE BEST TRANSDUCER POWER GAIN $T(\omega)$

Referring to Fig.6 and Fig.7, let $T(\omega)$ be the transducer power gain (*TPG*) of the virtually matched system as specified by (8), which is optimized over the specified normalized angular frequency bandwidth B such that $B = [\omega_{c2} - \omega_{c1}]$.

Let T_{min} be the minimum of $T(\omega)$ in B. Let T_{max} be the maximum of $T(\omega)$ in B. Let $T_{mean} = \frac{T_{max}+T_{min}}{2}$ be the mean value of $T(\omega)$ in B and let $\Delta T = T_{max} - T_{mean} = T_{mean} - T_{min}$ be the gain fluctuation in B. By trial and error, one can determine a flat gain level T_0 in such a way that T_{min} reaches to its maximum value in B. **This state of** *TPG* **is called the "RFLST based power delivery/intake performance, of the given complex immittance** $K(j\omega)$ **over the specified bandwidth** B. In this state, the mean value of the transducer power gain describes the average value of the power transfer with optimum fluctuations. In this state, *TPG* may be expressed as $T\,(\omega) = T_{mean} \mp \Delta T$. During the minimization process of (9), T_0 may be swept starting from the flat gain level $T_0(1) = 0.60$ upto unity $T_0(n_k) = 1$ with small step sizes δT. For example, δT may be selected as $\delta T = 0.05$. In this case, we define an index k in a loop to minimize the error function $\varepsilon(\omega, T_0(k))$ of (9) for a total number $n_k + 1 = 9$ times. Then, at each step k, we store $K_Q\,(j\omega, k) = R_Q\,(\omega, k) + jX_Q(\omega, k)$, $T_{min}(k)$, $T_{max}(k)$, $T_{mean}(k)$, $\Delta T(k) T(\omega, k)$ and $T_0(k)$ to determine the optimum "**gain − state**" yielding the "**RFLST based Power Delivery/Intake Performance**" of the complex termination $K\,(j\omega) = R\,(\omega) + jX(\omega)$ over B, which in turn results in the best Realizable-Driving Point Input Immittance in the form of line segments or equivalently as sampled data points.

For all the nonlinear optimization problems, initialization of the knowns is always crucial. Therefore, in the next subsection, we present a rule of thumb to initialize the unknown break points R_j for the minimization of the error function $\varepsilon(\omega, T_0(k))$ at a fixed flat gain level T_0.

B. INITIALIZATION OF THE NONLINEAR MINIMIZATION PROCESS

Before we introduce the optimization process, for a selected flat gain level T_0 and normalized break frequencies $\{\omega_1, \omega_2, \omega_3, \ldots \omega_N\}$, the unknown break points $\{R_1, R_2, R_3, \ldots R_N\}$ must be initialized. In this regard, initialization of the break points can be performed using (8) by assuming reactance cancellation. In other words, to maximize $T(\omega)$ of (8), the reactance term $(X_Q - X)$ is set to zero to derive the initials break points R_{int-j} such that

$$T_0 \approx \frac{4R_Q R}{\left[R_Q + R\right]^2} \tag{10a}$$

or

$$R_{int-j} = R\left(\omega_j\right)\left[\frac{2 - T_0 + 2\mu\sqrt{1 - T_0}}{T_0}\right] \geq 0 \tag{10b}$$

In (10b), μ is a unimodular constant. It is set to $\mu = +1$ for the high values of initials R_{intH-j} or it is selected as $\mu = -1$ for the low initials R_{intL-j}.

C. MINIMIZATION OF THE ERROR FUNCTION

We use MATLAB's nonlinear equation solver which is called "*lsqnonlin*" to minimize the sum of square errors ϵ such that

$$\epsilon = \sum_{r=1}^{N_S} [\varepsilon(\omega_r, R_1, R_2, R_3, \ldots, R_{N-1})]^2\,; \quad \omega_{c1} \leq \omega_r \leq \omega_{c2} \tag{11}$$

In (11), the integer N_S is the total number of sampling points over the passband $B = [\omega_{c2} - \omega_{c1}]$ subject to minimization. The normalized angular frequencies ω_{c1} is the low-end and ω_{c2} is the high-end of the frequency band. Thus, the unknown break points $x = \{R_1, R_2, R_3, \ldots, R_{N-1}\}$ are determined to minimize the sum of squares error ϵ. Minimization is performed using the Levenberg-Marquardt algorithm [24]–[26].

During minimization of sum of squares error, the first break point R_1 may be kept constant as it is initialized. This constant value may be zero for bandpass problems (i.e., $R_1 = 0$) or it may be included among the unknown break points. At the end of the minimization process, the realizable-driving point input immittance $K_Q\,(j\omega) = R_Q\,(\omega) + jX_Q(\omega)$ is obtained, which is the optimum possible line-segment model for the measured immittance data $K(j\omega) = R(\omega) + jX(\omega)$.

Thus, using the above concepts we developed a MatLab program called

"*Main_PDI_CGF*40010*F_IMMITANCE_MODEL.m*".

This program generates the best transducer power gain for the optimum source/load immittances using the virtual matching problem of Fig.6. This process is called the "Virtual Gain Optimization" or in short VGO.

At this point, it is important to re-emphasize that the error function of (9b) is a convex function of the unknown break points R_i, regardless of what the total number of unknowns are. Therefore, global minimum of the error function is hit, which in turn yields the best solution for the selected flat gain level $T_0(k)$ over the passband. Thus, we say that **RF-LST never requires selecting a circuit topology nor an analytic form of a transfer function to optimize the transducer power gain of the matched structure under consideration. Hence, the ultimate gain-bandwidth limitation (GBWL) of the given source and load pull impedances are automatically determined. Eventually, RF-LST based optimum-realizable source/load pull impedances are obtained as the result of the minimization process.**

Now, let us implement the above minimization process to predict the power intake and power delivery performance of the source and the load pull impedances for the *Wolfspeed CGH40010F* power transistor.

V. THE POWER INTAKE PERFORMANCE OF A GaN DEVICE

In this section, we will investigate the "power-intake" capability of the *Wolfspeed CGH40010F GaN* transistor at its input [14]. Transistor is driven by a resistive generator of $R_0 = 50\,Ohm$. The given source-pull impedance is approximated as the driving-point back-end impedance of a lossless two-port [E] when it is terminated in the complex-conjugate of the given source pull immittance as in Fig.5a. In this regard, it is desired to determine the gain-bandwidth limitation of the given source-pull impedance as detailed in the above section. The given/augmented and the normalized source-pull impedances are depicted in Fig. 5a. User defined passband is specified over $f_{C1} = 800MHz$ and $f_{c2} = 3.0\,GHz$. In this case, we select the normalizing frequency F_0 at $3.0\,GHz$. The real part of the given source-pull impedance is augmented at DC (i.e., $f = 0$) as $RSA\,(1) = 25\Omega$ and $RSA\,(N) = 0\Omega$. Similarly, the given imaginary part XSA is augmented as $XSA(1) = 0$ at DC $(i.e. ws1 = 0)$ and the end point is augmented at 4 GHz as $XSA(N) = -13.6\Omega$.

The GBWL of the virtual matching problem of Fig. 5a is numerically assessed via RF-LST employing our MatLab program "*Main_PIP_CGH*40010*_SOURCEPULL_LST.m*". Inputs to the main program are summarized as follows.

$\omega_{C1} = \frac{0.8}{F0} = 0.2667$; $\omega_{C2} = \frac{3GHz}{F0} = 1$; $\omega_{s1} = 0$; $\omega_{s2} = \frac{4}{F0} = 1.333$. We have selected $N = 21$ break points with 19 unknowns. In the optimization process, we prefer to work with impedances. $RB1 = 0$ is fixed at DC, since we deal with a bandpass single matching problem. Flat gain levels are swept between 0.6 and 1.0 with $\delta T = 0.05$ incremental steps. Therefore, we define the total number of 9 flat gain levels. Eventually, we start the optimization with low initials by selecting $\mu = -1$.

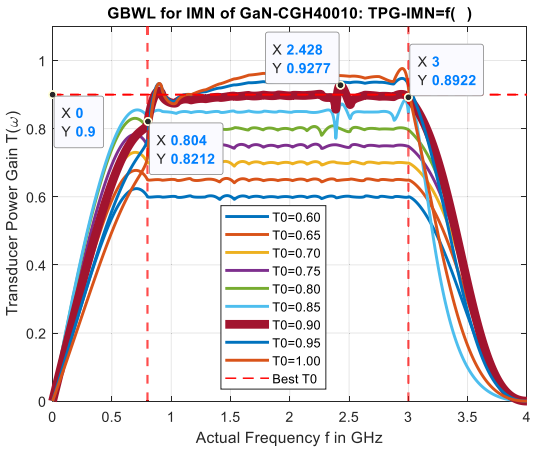

FIGURE 8. Power intake performance of the *GaN* device obtained by sweeping $T_0\,(k)$. It is noted that the best TPG is obtained for $T_0(7) = 0.9$.

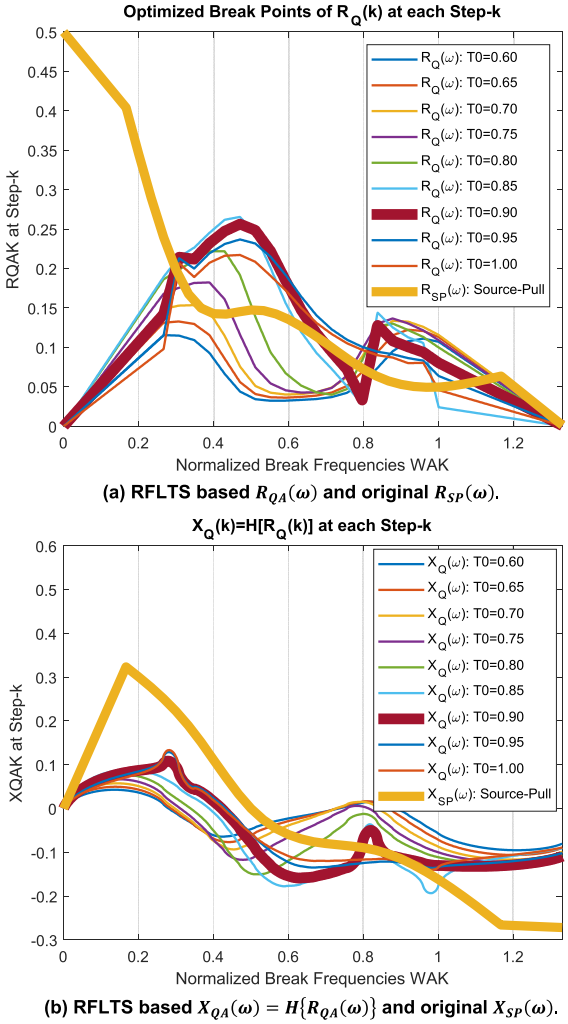

(a) RFLTS based $R_{QA}(\omega)$ and original $R_{SP}(\omega)$.

(b) RFLTS based $X_{QA}(\omega) = H\{R_{QA}(\omega)\}$ and original $X_{SP}(\omega)$.

FIGURE 9. Real and Imaginary parts of the RFLST based and original source pull impedance.

TABLE 1. Power-intake performance of the source-pull data CGH40010F power transistor.

$T_0(k)$	T_{mean}	F_max (GHz)	T_{max}	F_min (GHz)	T_{min}	ΔT
0.6000	0.5980	1.4720	0.6035	1.4080	0.5925	0.0055
0.6500	0.6476	1.4640	0.6539	1.5320	0.6412	0.0064
0.7000	0.6970	1.4560	0.7040	1.5320	0.6900	0.0070
0.7500	0.7483	2.2160	0.7546	2.2720	0.7420	0.0063
0.8000	0.7945	2.3640	0.8082	2.2680	0.7807	0.0137
0.8500	0.8280	2.9720	0.8841	2.3880	0.7719	0.0561
0.9000	0.8745	2.4280	0.9277	0.8040	0.8212	0.0532
0.9500	0.8656	2.9480	0.9477	0.8040	0.7835	0.0821
1.0000	0.8559	2.9480	0.9768	0.8040	0.7350	0.1209

TABLE 2. Power-delivery performance of the load-pull data CGH40010F power transistor.

$T_0(k)$	T_{mean}	F_max (GHz)	T_{max}	F_min (GHz)	T_{min}	ΔT
0.6000	0.6003	2.9440	0.6023	3.0000	0.5983	0.0020
0.6500	0.6503	2.9400	0.6536	3.0000	0.6470	0.0033
0.7000	0.7000	2.9360	0.7060	3.0000	0.6940	0.0060
0.7500	0.7483	2.9240	0.7612	3.0000	0.7354	0.0129
0.8000	0.7883	2.9040	0.8234	3.0000	0.7532	0.0351
0.8500	0.7995	2.8840	0.8871	3.0000	0.7119	0.0876
0.9000	0.7883	2.8800	0.9176	3.0000	0.6590	0.1293
0.9500	0.7747	2.8760	0.9225	3.0000	0.6269	0.1478
1.0000	0.7631	0.9200	0.9191	3.0000	0.6071	0.1560

Results of the sequential optimization of *TPG* are summarized as in Table 1 and depicted as in Fig. 8. The best performance appears for $\max(T_{min}) = 0.8212$ or equivalently, $T_{mean} = 0.8745 \mp 0.0532$. Optimized break points R_{QLST-S} and its corresponding Hilbert Transform X_{QLST-S} are depicted in Fig. 9a and 9b respectively as compared with the manufacturer's published source pull data.

Referring to Table 1 and Fig. 8, it is predicted that 87.45% of the available power of the generator is transferable to the input of the power transistor *CGH*40010F with optimum fluctuation of $\Delta T = \mp 0.0532$ in least mean square sense. Let us now investigate the output power delivery performance of the same transistor using the load-pull measured impedance data in the following section.

VI. THE POWER DELIVERY PERFORMANCE OF A GaN DEVICE

In this section, we will investigate the power delivering capability of the *WolfspeedCGH*40010*F GaN* transistor at its output-port [14]. Here, we assumed that the transistor is terminated in its modelled-realizable optimum-load-pull impedance over the output matching network (OMN) while the other end of OMN is terminated in $R0 = 50\Omega$. The measured load-pull impedance is approximated as the driving-point backend impedance of a lossless two-port [E] when it is terminated in the complex-conjugate of the load pull immittance as in Fig. 5b.

In the performance assessment computations, user defined passband is selected as before with $F_0 = 3.0\,GHz$. The real part of the measured load-pull impedance is augmented at DC (i.e., $f = 0$) as $RLPA\,(1) = 61\Omega$ and $RLPA\,(N) = 0\Omega$. Similarly, the measured imaginary part *XLPA* is augmented as $XLPA(1) = 0$ at *DC* $(i.e. ws1 = 0)$ and the end point is augmented at 6GHz as $XLPA\,(N) = +11\Omega$ $(i.e., ws2 = 4/F0 = 1.333)$.

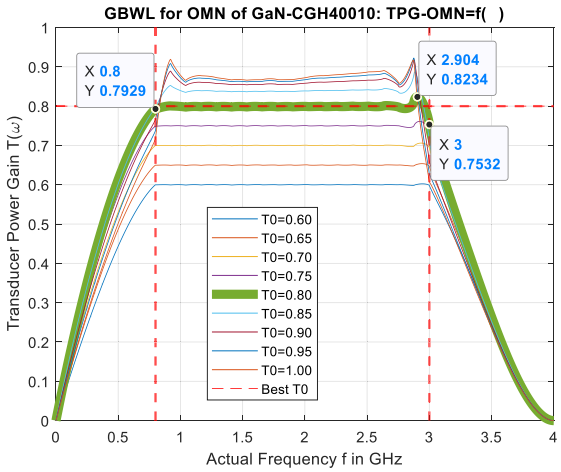

FIGURE 10. Power delivery performance of the GaN device obtained by sweeping $T_0(k)$. It is noted that the best TPG is obtained for $T_0(5) = 0.8$.

Execution of our MatLab program "*Main_PDP_CGH*40010*_LADPULL_RFLST.m*" results in the RF-LST based Gain Bandwidth Limitation of the load pull impedance. Results of the sequential optimization of *TPG* are summarized as in Table 2 and depicted as in Fig. 10. The best performance appears for $\max(T_{min}) = 0.7532$ or equivalently, $T_{mean} = 0.7883 \mp 0.0351$. Optimized break points R_{QLST-L} and its corresponding Hilbert Transform X_{QLST-L} are depicted in Fig. 11a and 11b respectively as compared with the manufacturer's published load pull impedance data.

Referring to Table 2 and Fig. 10, it is predicted that 78.83% of the output power is delivered to the load pull impedance of the power transistor *CGH*40010. In other words, power delivery performance of the optimum realizable load pull impedance is $T_{mean} = 0.7883$ with corresponding fluctuation of $\Delta T = \mp 0.0351$.

VII. GENERATION OF AN ANALYTIC MODEL FOR THE GIVEN IMMITTANCE DATA

In the previous sections, power-intake and power delivery performance of the optimum-realizable source and load pull immittances are determined using the real frequency-line segment technique (RF-LST). The follow-up step should be to build the best analytic immittance models for the RF-LST based terminations so that the input and the output matching networks are constructed. In this regard, the VGO method is adopted to build the analytic model for the given minimum immittance data. Referring to Fig.6, the load termination $K_{LA}\,(j\omega) = R_{LA}\,(\omega) + jX_{LA}(\omega)$ is described as the complex conjugate of the minimum immittance data

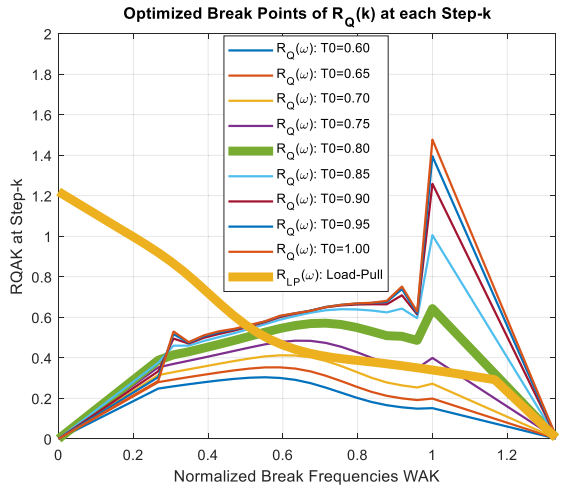

(a) RFLTS based $R_{QA}(\omega)$ and original $R_{LP}(\omega)$.

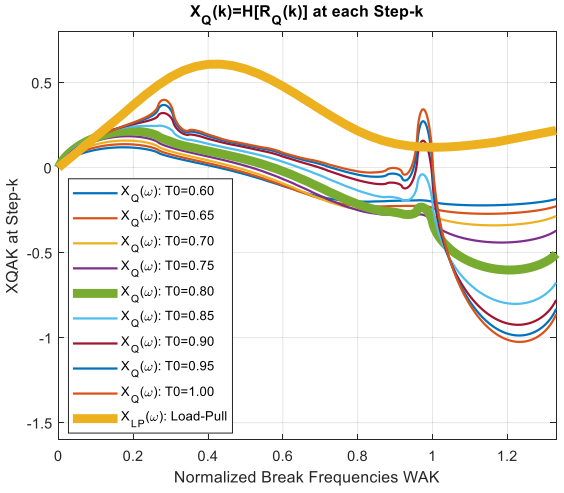

(b) RFLTS based $X_{QA}(\omega) = H\{R_{QA}(\omega)\}$ and original $X_{LP}(\omega)$.

FIGURE 11. Real and Imaginary parts of the RFLST based and original load pull impedance.

$KA(j\omega) = RA(\omega) + jXA(\omega)$ such that

$$R_{LA}(\omega) = RA(\omega) \tag{12a}$$

$$X_{LA}(\omega) = -XA(\omega) \tag{12b}$$

Thus, the transducer power gain is given by

$$T(\omega) = \frac{4R(\omega)RA(\omega)}{[R(\omega) + RA(\omega)]^2 + [X(\omega) - XA(\omega)]^2} \tag{13}$$

In (13), the realizable-rational real part function $R(\omega) = R\left(p^2\right)|_{p^2=-\omega^2}$ is described in terms of an auxiliary polynomial $c(\omega) = c_1\omega^n + c_2\omega^{n-1} + \ldots + c_n\omega + 1$ such that

$$R(\omega) = \frac{a_0^2(-1)^{ndc}\omega^{2ndc}\prod_{i=1}^{nr}\left(\sigma_i^2 + \omega^2\right)^2\prod_{j=1}^{nz}\left(\omega_i^2 - \omega^2\right)^2}{B\left(\omega^2\right)} \tag{14a}$$

where

$$B\left(\omega^2\right) = \frac{1}{2}\left[c^2(\omega) + c^2(-\omega)\right] > 0; \quad \forall\omega \tag{14b}$$

In the above formulations, n is the degree of the auxiliary polynomial which corresponds to the total number of the reactive components in the matching network when the modelled immittance is synthesized as a lossless two-port in Darlington sense. The integer *ndc* is the count for the total number of transmission zeros at DC. The symbol σ_i is a positive real number referring to Right Half Plane (RHP) transmission zeros. The symbol ω_i designates the finite transmission zeros on the frequency axis $j\omega$ as it comes with its complex conjugate pair. From the programming point of view, all the RHP zeros and finite frequency transmission zeros may be collected under vectors $S = [\sigma_1, \sigma_2, \cdots, \sigma_{nr}]$ and $W = [\omega_1, \omega_2, \cdots, \omega_{nz}]$ respectively. It should be emphasized that a for typical matching network, all the transmission zeros are selected by the designer as the input to the VGO program since they impose the topological structure of the matching network. In this regard, unknowns of the virtual gain optimization are selected as the real coefficients $\{c_1, c_2, c_3, \ldots, c_n\}$. The real constant a_0 may as well be included among the unknowns. Once a_0 and $\{c_1, c_2, c_3, \ldots, c_n\}$ are initialized, the analytic form of the minimum immittance $K(p) = \frac{a(p)}{b(p)}$ is generated using the parametric approach [19], [20], [27]–[29]. Eventually, for a selected constant flat gain level T_0, the error function

$$\begin{aligned}\varepsilon(\omega, c_1, c_2, c_3, \ldots, c_n, a_0) &= T(\omega) - T_0 \\ &= \frac{4R(\omega)RA(\omega)}{[R(\omega) + RA(\omega)]^2 + [X(\omega) - XA(\omega)]^2} - T_0\end{aligned} \tag{15}$$

is minimized over the passband. In (15), T_0 may be set to unity since a good fit between the pairs $\{R(\omega), X(\omega)\}$ and $\{RA(\omega), XA(\omega)\}$ is sought. For the sake of completeness, let us summarize the parametric approach to construct a positive real immittance function $K(p)$ from its even part $R(\omega)$ as specified by (14).

VIII. A PARAMETRIC METHOD TO BUILD A PR MINIMUM FUNCTION $K(p)$ FROM ITS EVEN PART $R\left(p^2\right)$

In this method, a minimum positive function $K(p)$ is expressed in terms of its LHP poles p_i as follows [19], [20], [27]–[29].

$$K(p) = \frac{a(p)}{b(p)} = R_\infty + \sum_{j=1}^{n}\frac{k_j}{p - p_j} \tag{16a}$$

The above form is called the parametric representation of a minimum positive real function $K(p)$.

Similarly, even part $R(p^2)$ of $K(p)$ is also expressed in parametric form as

$$R(p^2) = \frac{1}{2}[K(p) + K(-p)] = R_\infty + \sum_{j=1}^{n}\frac{k_j p_j}{p^2 - p_j^2} \tag{16b}$$

where the residues are given by

$$k_j = \left(p^2 - p_j^2\right)\frac{R\left(p_j^2\right)}{p_j}$$

$$= \frac{A(p_j^2)}{(p_j)(-1)^n (c_1^2) \prod_{\substack{i=1 \\ i\neq j}}^{n} p^2 - p_i^2} \tag{16c}$$

$$R_\infty = R\left(p^2\right) \tag{16d}$$

Once the transmission zeros are selected, the arbitrary real coefficients $\{c_i; i = 1, 2, .., n\}$ and a_0 are initialized, then even denominator polynomial $B(\omega^2)$ of (7b) are computed as

$$B\left(\omega^2\right) = \frac{1}{2}\left[c^2(\omega) + c^2(-\omega)\right] = B_1\omega^{2n} + B_2\omega^{2(n-1)} + \ldots + B_n\omega^2 + 1 > 0\forall\omega \tag{16e}$$

Afterwards, $B(p^2)$ is generated replacing ω^2 by $-p^2$. At this point, mirror-image symmetric roots of $B(p^2)$ are computed. For example, on MatLab, the command $x = roots(B)$ returns all the roots of the denominator polynomial $B(x)$ with $x = p_i^2$. Then, we set $p_i = \mp\sqrt{x}$. Let the roots of $B(p^2)$ are designated by $p = \mp p_i$; $i = 1, 2, \ldots, n$. Selecting LHP roots p_j of $B(p^2)$, denominator polynomial $b(p)$ of $Z(p) = \frac{a(p)}{b(p)}$ is constructed as

$$b\,(p) = |c_1| \prod_{j=1}^{n} (p + p_j) \tag{16f}$$

Using (16c) and (16d), the residues k_j and R_∞ are computed. Then, $K(p)$ is generated as in (16a). Finally, its rational form is determined by algebraic manipulations to end up with the rational form of $K\,(p) = a(p)/b(p)$. In (16f), $b(p)$ is a strictly Hurwitz real polynomial. Therefore, complex roots of $b(p)$, which are specified by $p_j = -\sigma_j + j\omega_j$; $\sigma_j > 0$, must be accompanied with its complex conjugate pairs such that $p_{j+1} = -\sigma_j - j\omega_j$; $j = 1, 2, \ldots, n$. Thus, once the transmission zeros are selected (i.e. ndc, $W = [\omega_1, \omega_2, \cdots, \omega_{nz}]$ and $S = [\sigma_1, \sigma_2, \cdots, \sigma_{nr}]$) and the coefficients a_0 and $\{c_1, c_2, c_3, \ldots, c_n\}$ of the auxiliary polynomial is initialized, minimum function $K\,(p) = a(p)/b(p)$ is generated employing (16). Hence, minimization of the error function of (15) results in the analytic form of $K\,(p) = \frac{a(p)}{b(p)} = \frac{a_1p^n + a_2p^{n-1} + a_3p^{n-2} + \ldots + a_np + a_{n+1}}{b_1p^n + b_2p^{n-1} + b_3p^{n-2} + \ldots + b_np + 1}$ as in (16). It is noted that in our computations, we take $a_1 = 0$ since $R(p) = 0$ is assumed. Furthermore, in MatLab computations, a polynomial $a(p)$ of degree n is defined as a vector $a = [a_1a_2 \ldots a_{n+1}]$ of n+1 tuples.

Eventually, $K\,(p) = \frac{a(p)}{b(p)}$ is synthesized as a lossless two-port in Darlington sense. If $K\,(p)$ refers to the source/load pull immittance, the lossless two-port will be the input/output matching network. Optimization and Synthesis are implemented under MatLab environment in a similar manner to that of [30]–[34].

IX. ANALYTIC MODELS FOR THE RF-LST BASED SOURCE AND LOAD IMPEDANCES

In Section V and VI, Power-Intake and Power-Delivery Performance of the device is obtained over the given source/load pull impedance data. In this section, we build practical analytic models for both source and load pull impedances as follows.

TABLE 3. Optimized analytic impedance function $Z_{QA-S}\,(p) = a(p)/b\,(p)$ which best fits the RFLST based source-pull impedance $Z_{QLST-S}\,(j\omega) = R_{QLST-S}\,(\omega) + jX_{QLST-S}(\omega)$.

For Nc=5; ndc=1	
a_{0G}	2.1208
$c(\omega)$	[−16.2278 1.5185 21.6723 4.1441 − 2.3591]
$a(p)$	[0 1.5239 1.6028 2.1996 0.9545 0]
$b(p)$	[16.2278 17.0679 30.5770 17.6893 7.0166 1.0000]

For Nc=8; ndc=2	
a_{0G}	2.3455
$c(\omega)$	[15.86 − 69.77 − 38.85 78.31 28.50 − 12.57 − 13.86 − 1.02]
$a(p)$	[0 1.2083 6.4653 8.1143 8.7234 5.7561 1.9264 0.3930 0]
$b(p)$	[15.86 84.84 112.32 145.75 113.51 60.67 25.35 4.90 1.00]

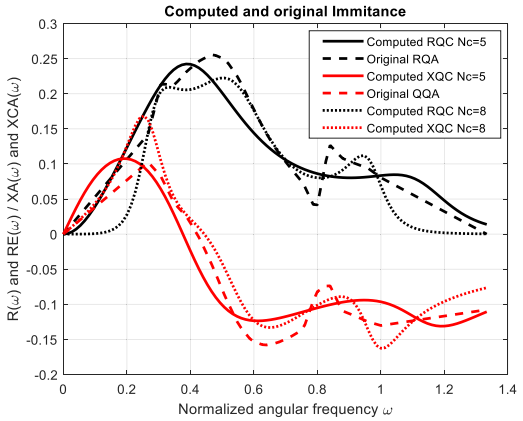

FIGURE 12. Fit between the modeled and RF-LST based source impedance real and imaginary parts.

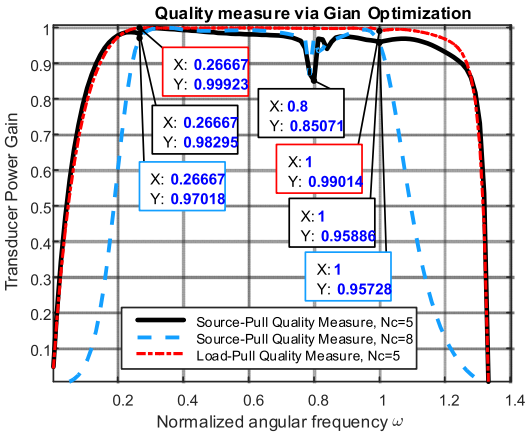

FIGURE 13. Quality measure for the fit between optimum and modeled impedances via VGO algorithm.

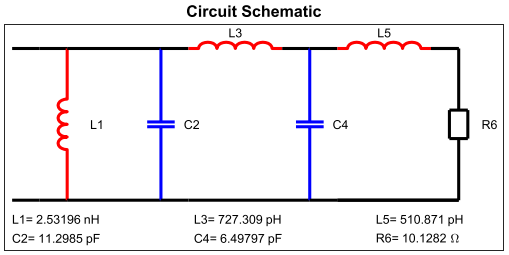

(a) 5 element network with ndc=1.

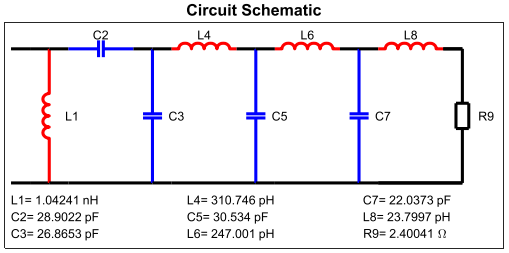

(b) 8 element network with ndc=2.

FIGURE 14. Synthesized networks by modeling the RF-LST based source impedance.

A. SOURCE-PULL IMPEDANCE MODEL

RF-LST based optimum source impedance data is shown Fig.9 as yellow plot. Employing the modelling method introduced above, we obtained the realizable analytic form for the optimum source impedance $Z_{QA-SP}(p) = a(p)/b(p)$ as specified in Table 3 for $n = 5$ and $ndc = 1$ (a single transmission zero at dc). Data fit between the analytic impedance and the RF-LST based source impedance data are depicted in Figure 12. In this regard, quality of the curve fitting (QF) may be evaluated by means of the virtual transducer power gain (VTPG). For example, VTPG=1 corresponds to exact fit at the given points over the passband. Otherwise, trace of the analytic function will deviate from the original RF-LST points. VTPG of the IMN is depicted in Fig. 13 with the black curve. Close examination of this figure reveals that quality of match is about 95% but it drops down to 85% in the vicinity of the normalized frequency $\omega = 0.8$. The analytic form of $Z_{QA-SP}(p) = a(p)/b(p)$ is synthesized as in Fig. 14. Synthesis is completed using our "high-precision Darlington synthesis (HPDS) methods" presented in [30]–[34]. In HPDS, driving point input immittance is corrected after each transmission zero extraction. In this way, one can synthsize a lossless matching network with more than 30 reactive elements with relative error less than 10^{-4} as reported in [30]–[34]. The alternative sysnthesis could be to use Darlington Synthesis in a straight forward manner without immittance correction. In this way, sythesis is halted after a few steps due to overflow/underflow errors occour during the computations. Another high precision synthesis method is reported in [35], which utilized the correction on the Feldkeller condtion after each transmission zeros extranction. However, this work is only good for lowpas LC ladder synthesis, and the resulting computational precion is

TABLE 4. Optimized analytic impedance function $Z_{QA-L}(p) = a(p)/b(p)$ which best fits the RFLST based load-pull impedance $Z_{QLST-L}(j\omega) = R_{QLST-L}(\omega) + jX_{QLST-L}(\omega)$.

a_{0L}	4.0827
$c(\omega)$	[3.7719 0.9181 − 0.6221 3.5809 − 4.2652]
$a(p)$	[0 1.3928 3.9380 4.7844 2.8723 0]
$b(p)$	[3.7719 10.6645 15.5864 15.2137 7.4687 1.0000]

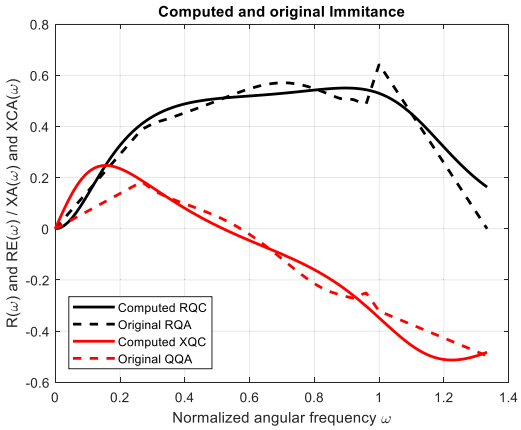

FIGURE 15. Fit between the modeled and RF-LST based load impedance real and imaginary parts.

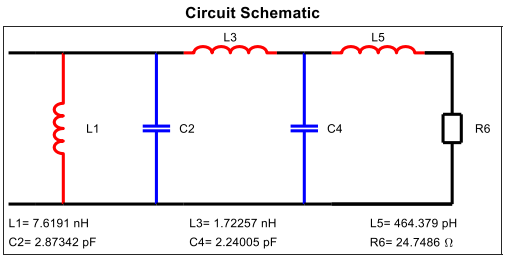

FIGURE 16. Synthesized network by modeling the RF-LST based load impedance.

similar to that of [30]–[34] upto 10 elements. It should be mentioned that QF may be improved by increasing the total number of elements in the matching networks. For example, In Table 3, we present the results of VTPG optimization for $ndc = 2, Nc = 8$ case. Corresponding VTPG is also depicted in Fig.13 with blue dashed plot. As it is seen from Fig.13, quality of fit is slightly improved with sharpened edges. Nevertheless, for the sake of simplicity, we have selected the "5 element IMN" to construct PA.

B. LOAD-PULL IMPEDANCE MODEL

In Fig.11, RF-LST based load-pull impedance data is depicted (green plot). Utilizing the analytic virtual modeling method, we end up with the positive-real function form for the load pull impedance as listed by Table 4 for $ndc = 1$ and $n = 5$. The fit between the analytic form and the break points are shown in Fig. 15. Quality of fit (QF) is depicted

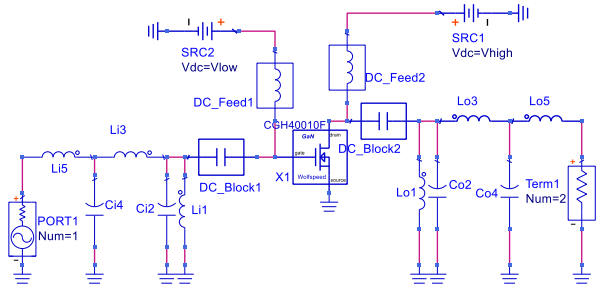

FIGURE 17. ADS simulation schematic of the designed amplifier.

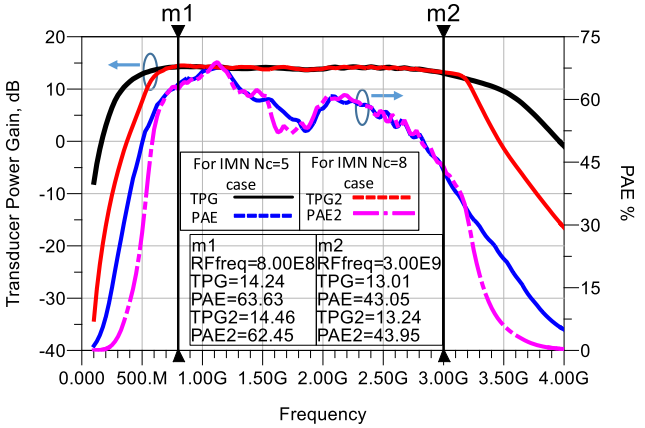

FIGURE 18. ADS simulation results of the designed amplifier.

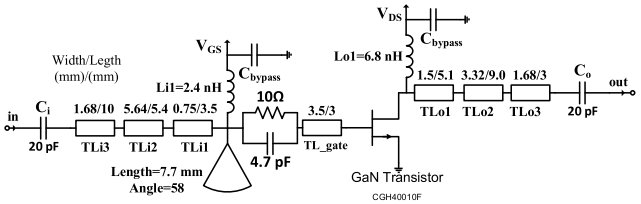

FIGURE 19. Converted mixed equivalent of the designed amplifier.

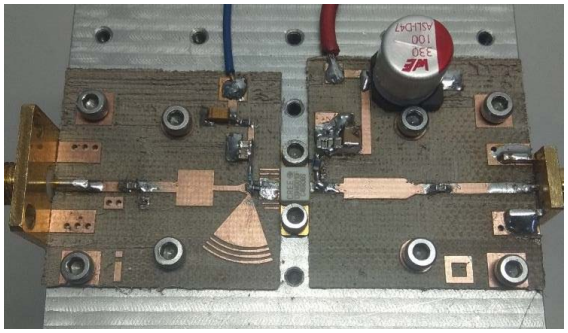

FIGURE 20. Photo of the prototype amplifier.

in Fig. 13 with the red-dotted curve. Here in this case, QF is better than 99% over the entire frequency band. Hence, synthesis of $Z_{QA-LP}(p) = a(p)/b(p)$ is shown in Fig 16.

Note that, it is possible to build an exact model for the RF-LST based immittance data yielding perfect match employing the linear interpolation method of positive real functions [36]. However, this method unnecessarily complicates the matching network topology with total number of $2(N-1)$ components. In this representation, integer N refers to the count of sampling points as in Fig.2.

X. SIMULATION OF THE PA WITH SYNTHESIZED MATCHING NETWORKS

In this section, we carried out the simulation and re-optimization process of the designed power amplifier using ADS as depicted in Fig.17 [37]. The circuit components of the IMN (Fig.14) and OMN (Fig.16) are re-optimized to improve the TPG and the power added efficiency of the overall amplifier to end up with practically implementable component values. Finally, the amplifier is manufactured, and its performance is measured. Details are summarized as follows.

In Fig.17, for AB-Class operation, the *GaN* transistor CGH40010F is biased with $VDD = 28\ Volts$, $VGG = -2.82\ Volts$, $IDD = 150\ mA$. Over the passband, driving input power of the amplifier is kept constant at $P_{in} = 28\ dBm$ level. Under the above conditions, simulation results are given in Fig.18. Close examination of this figure reveals that the average value of TPG is 13.6 dB with ∓ 0.6 dB fluctuation and the PEA varies between 65% down to 43% over the passband of (800MHz-3GHz). For the sake of comparison, simulation results for the synthesized IMN with $Nc = 8$ elements, is also depicted in Fig 18 as TPG2 and PAE2. As can be seen from this figure, the passband performance is similar to that of 5 element IMN, whereas the stop-band roll-offs is sharpened as expected.

So far, we are only concerned with the optimum data fit between the realizable analytic forms and the given source/load-pull immittance data. Therefore, we did not care about the IMN and OMN resistive terminations if they are 50 ohms or not. As a matter of fact, they are also included among the unknowns of the virtual matching problems by varying the real constant a_0 of (14a). Indeed, for IMN, the optimum solution is obtained for $a_{0G} = 2.12$ which yields $R_{0G} = 10.13\Omega$. Similarly, the terminating resistor of OMN is $R_{0L} = 24.75$ which refers to the real constant $a_{0L} = 4.08$. However, practical designs of IMN/OMN may require 50Ω terminations. This fact can be taken care of in ADS during the re-optimization process. Moreover, for the sake of simple PA fabrication, most of the lumped elements are converted to microstrip lines. Thus, we end-up with the final design as depicted in Fig. 19. At this point, it is crucial to emphasized that, without using VGO method, which yields the circuit topologies with element values for IMN and OMN as depicted in Fig.14 and Fig.16, we would not be able to carry-out the re-optimization to end-up with the final design of the PA on ADS as depicted in Fig.19.

Referring the Fig.17 and Fig. 19, capacitors and inductors can be realized as cascaded microstrip lines. The shunt

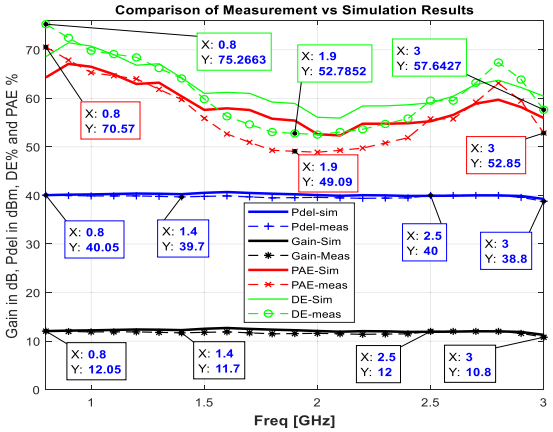

FIGURE 21. Measurement vs simulation results.

TABLE 5. Comparisons with the recently published PAs.

[Ref]-[Year]	Frequency Band GHz	Gain (dB)	Pout(dBm)	*DE*/PAE [%]
[1]-[2022]	0.5-2.8	10-12	40-42.5	*DE*: 63-69
[2]-[2018]	1.2-3.6	10.5-12.5	40-42.2	*DE*: 60-72
[3]-[2017]	1.8-2.7	9.6-11.2	39.5-42	*DE*: 64-81
[4]-[2016]	0.6-3.8	9-14	40-41.9	PAE: 46-75
[5]-[2016]	0.8-3.05	9.8-13.2	40-43.2	*DE*: 57.4-79.1
[6]-[2014]	1.6-2.8	11.9-15.2	40-42.5	*DE*: 67.5-81.9
This work [2022]	0.8-3.0	10.8-12.05	38.8-40.05	*DE*: 52.8-75.3 PAE: 49-70.6

inductors L_{i1} of IMN and L_{o1} of OMN are connected through the bias lines. Due to its substantial value, it is appropriate to realize the capacitor C_{i2} of IMN as a radial stub. After re-optimization, it is found that, inductors L_{i5}, L_{o5} and the capacitor C_{o2} can be disregarded due to their negligible contributions to the PA performance. The series inductors L_{i3} and L_{o3} are printed on the top surface as transmission lines TL_{i1} and TL_{o1} respectively. In a similar manner, C_{i4} of the IMN is realized as TL_{i2}. The pi section $[C_{o2} - L_{o3} - C_{o4}]$ of Fig. 17 can be replaced with a single transmission line TL_{o2} as described in [38]–[41]. Additionally, required connection lines such as bias and solder paths for gate/drain leads of the active device are inserted. Furthermore, an RC low-frequency damping circuit is included to compensate low frequency gain variations, to reduce the return loss and to improve the stability of the amplifier. As a substrate, Taconic RF35 board is used for the PA realization with dielectric constant $\epsilon = 3.5$ and $h = 30mil$ thickness [42]. Non-ideal discrete component models are inserted for lumped elements (i.e. for C_i and C_o, 600S series from Kyocera AVX corp. for C_G and $Li1$, GJM15 and LQW15 series from Murata respectively and for $Lo1$, 603HP series from coil-craft [43]–[45]). After these modifications, EM analysis and post-layout optimizations are completed with the best possible realizable form of the amplifier. The finalized schematic of the amplifier is given in Fig. 19. The picture of the manufactured amplifier is given in Fig. 20. The final simulation and the measurement results are given in Fig 21. As it is seen from the figure, the actual TPG is 11.4 ± 0.6 dB, PAE varies between 49% up to 71% and the drain efficiency (DE) varies between 52.8% and 75.3%.

At this point, it is useful to compare the measured performance of our amplifier with similar PAs, listed in Table 5. It is unveiled that, our newly proposed VGO neither requires selection of matching network topology nor demands the initialization of the element values. They are the results of the VGO method introduced in this paper. Furthermore, our PA offers the minimum fluctuations within high average TPG with minimum fluctuations in broadband.

XI. CONCLUSION

This research work proposes a structured set of sequential procedures to design power amplifiers. The power amplifier design process starts with the selection and characterization of an active device which must provide the desired output power level in demand over a prescribed frequency band. The active device may be a *GaN* power transistor. In this regard, the source/load pull impedances of the active device are generated to optimize the power added efficiency (PAE), and transducer power gain (TPG) while minimizing the harmonics of the amplifier over the frequency band of interest. At this point, it is crucial to note that for many practical situations, source and load pull impedances placed on the Smith Chart, do not necessarily belong to realizable positive functions (PR) over the passband. In this case, one must check if these impedances are realizable. If not, it is well known that power intake and power delivery performance of the active device is penalized heavily. Therefore, in this paper, we developed a test procedure to determine whether the given source and load pull data are realizable network functions. Then, we introduced a new numerical method to assess the Power Intake/Delivery Performance of the given source and load pull impedances employing the real frequency line segment technique. Thus, ultimate power intake and power delivery capacity of the nonlinear active device is determined. Then, we proposed an algorithm to generate the optimum-realizable source and load pull impedances as sampled data using the real frequency line segment technique, which in turn results in the numerical Power-Intake and Power-Delivery Performance of these impedances. Then, we generated positive real function models for the line segment based realizable optimum source and load pull impedance data, which results in the optimum input and output matching network topologies with component values. The proposed modelling algorithm employs the method, what we call is the "virtual gain optimization, VGO". Modelled positive real functions are synthesized as the front-end and the back-end lossless matching networks, yielding the optimum power added efficiency and the transducer power gain for the power amplifier under consideration. Eventually, component values of the resulting input and output matching networks are re-computed to

improve the electrical performance of the power amplifier employing a commercially available design packages such as ADS. Using *GaN* CGH40010F transistor, Using the proposed sequential design method step by step, we constructed an AB-Class power amplifier over $800MHz - 3GHz$ bandwidth. It is shown that the designed power amplifier offers 38.8dBm to 40.05 dBm output power, maximum of 70.6% at 800 MHz and a minimum of 49% at 3.0 GHz power added efficiency with a nearly flat transducer power gain of $T = 11.4 \pm 0.6dB$ over the 800MHz-3GHz bandwidth.

ACKNOWLEDGMENT

It is noted that this research work is completed under the Ph.D. thesis requirements of Sedat Kilinc at Istanbul Technical University under the supervision of Prof. Dr. Binboga Siddik Yarman and Prof. Dr. Serdar Ozoguz.

The authors thank Dr. Koray Gurkan of Istanbul University-Cerrahpaşa for his invaluable support in the manufacturing of the printed circuit board of the prototype power amplifier.

REFERENCES

[1] G. Liu, Z. Lai, G. Zhou, and Z. Cheng, "Design of a multi-octave power amplifier with a novel broadband design methodology," *IEICE Electron. Exp.*, vol. 19, no. 7, Apr. 2022, Art. no. 20220073, doi: 10.1587/elex.19.20220073.

[2] C. Huang, S. He, W. Shi, and B. Song, "Design of broadband high-efficiency power amplifiers based on the hybrid continuous modes with phase shift parameter," *IEEE Microw. Wireless Compon. Lett.*, vol. 28, no. 2, pp. 159–161, Feb. 2018, doi: 10.1109/LMWC.2017.2787061.

[3] X. Hu, X. Meng, C. Yu, and Y. Liu, "Design of highly efficient broadband harmonic-optimised GaN power amplifier via modified simplified real frequency technique," *Electron. Lett.*, vol. 53, no. 21, pp. 1414–1416, Oct. 2017. [Online]. Available: https://digital-library.theiet.org/content/journals/10.1049/el.2017.2849

[4] J. J. M. Rubio, V. Camarchia, R. Quaglia, E. F. Angarita Malaver, and M. Pirola, "A 0.6–3.8 GHz GaN power amplifier designed through a simple strategy," *IEEE Microw. Wireless Compon. Lett.*, vol. 26, no. 6, pp. 446–448, Jun. 2016, doi: 10.1109/LMWC.2016.2549263.

[5] W. Shi, S. He, Q. Li, T. Qi, and Q.-A. Liu, "Design of broadband power amplifiers based on resistive-reactive series of continuous modes," *IEEE Microw. Wireless Compon. Lett.*, vol. 26, no. 7, pp. 519–521, Jul. 2016, doi: 10.1109/LMWC.2016.2574823.

[6] J. Chen, S. He, F. You, R. Tong, and R. Peng, "Design of broadband high-efficiency power amplifiers based on a series of continuous modes," *IEEE Microw. Wireless Compon. Lett.*, vol. 24, no. 9, pp. 631–633, Sep. 2014, doi: 10.1109/LMWC.2014.2331457.

[7] G. R. Nikandish, R. B. Staszewski, and A. Zhu, "A fully integrated GaN dual-channel power amplifier with crosstalk suppression for 5G massive MIMO transmitters," *IEEE Trans. Circuits Syst. II, Exp. Briefs*, vol. 68, no. 1, pp. 246–250, Jan. 2021, doi: 10.1109/TCSII.2020.3008365.

[8] B. Liu, C. C. Boon, M. Mao, P. Choi, and T. Guo, "A 2.4–6 GHz broadband GaN power amplifier for 802.11ax application," *IEEE Trans. Circuits Syst. I, Reg. Papers*, vol. 68, no. 6, pp. 2404–2417, Jun. 2021, doi: 10.1109/TCSI.2021.3073345.

[9] A. Grebennikov, *Radio Frequency and Microwave Power Amplifiers: Principles, Device Modeling and Matching Networks*, vol. 1. London, U.K.: Institution of Engineering and Technology, 2019.

[10] R. S. Pengelly, S. M. Wood, J. W. Milligan, S. T. Sheppard, and W. L. Pribble, "A review of GaN on SiC high electron-mobility power transistors and MMICs," *IEEE Trans. Microw. Theory Techn.*, vol. 60, no. 6, pp. 1764–1783, Jun. 2012, doi: 10.1109/TMTT.2012.2187535.

[11] S. Mizuno, F. Yamada, H. Yamamoto, M. Nishihara, T. Yamamoto, and S. Sano, "Development of GaN HEMT for microwave wireless communications," *SEI Tech. Rev.*, no. 74, pp. 71–74, 2012.

[12] T. Kikkawa, K. Joshin, and M. Kanamura, "GaN device for highly efficient power amplifiers," *Fujitsu Sci. Tech. J.*, vol. 48, no. 1, pp. 71–74, 2012.

[13] K. Inoue, S. Sano, Y. Tateno, F. Yamaki, K. Ebihara, N. Ui, A. Kawano, and H. Deguchi, "Development of gallium nitride high electron mobility transistor for cellular base stations," *SEI Tech. Rev.*, no. 71, pp. 88–93, 2010.

[14] Wolfspeed and Cree Company, Durham, NC, USA. *GaN HEMT Transistor Series*. Accessed: Apr. 2022. [Online]. Available: https://www.wolfspeed.com/cgh40010

[15] T. Maier, V. Carrubba, R. Quay, F. van Raay, and O. Ambacher, "Active harmonic source-/load-pull measurements of AlGaN/GaN HEMTs at X-band frequencies," in *Proc. 83rd ARFTG Microw. Meas. Conf.*, Jun. 2014, pp. 1–4, doi: 10.1109/ARFTG.2014.6899516.

[16] V. Teppati, A. Ferrero, and M. Sayed, V. Teppati, A. Ferrero, and M. Sayed, Eds. *Modern RF and Microwave Measurement Techniques* (The Cambridge RF and Microwave Engineering Series). Cambridge, U.K.: Cambridge Univ. Press, 2013.

[17] S. C. Cripps, "A theory for the prediction of GaAs FET load-pull power contours," in *IEEE MTT-S Int. Microw. Symp. Dig.*, May/Jun. 1983, pp. 221–223, doi: 10.1109/MWSYM.1983.1130864.

[18] J. Cusack, S. Perlow, and B. Perlman, "Automatic load contour mapping for microwave power transistors," in *IEEE MTT-S Int. Microw. Symp. Dig.*, vol. 74, Jun. 1974, pp. 269–271, doi: 10.1109/MWSYM.1974.1123569.

[19] H. Carlin, "A new approach to gain-bandwidth problems," *IEEE Trans. Circuits Syst.*, vol. CAS-24, no. 4, pp. 170–175, Apr. 1977, doi: 10.1109/TCS.1977.1084325.

[20] B. S. Yarman, "Modern approaches to broadband matching problems: Real frequency solutions," in *Design of Ultra Wideband Power Transfer Networks*. Hoboken, NJ, USA: Wiley, 2010, ch. 11, pp. 539–586.

[21] B. S. Yarman, "Circuit theory for power transfer networks: Positive real functions," in *Design of Ultra Wideband Power Transfer Networks*. Hoboken, NJ, USA: Wiley, 2010, ch. 1, sec. 1.18, pp. 25–33.

[22] H. J. Carlin and P. P. Civalleri, *Wideband Circuit Design*. New York, NY, USA: CRC Press, 1998.

[23] MathWorks. *MATLAB Software*. Accessed: Apr. 2022. [Online]. Available: https://www.mathworks.com/products/MATLAB.html

[24] K. Levenberg, "A method for the solution of certain non-linear problems in least squares," *Quart. J. Appl. Math.*, vol. 2, no. 2, pp. 164–168, Jul. 1944. [Online]. Available: http://www.jstor.org/stable/43633451

[25] D. W. Marquardt, "An algorithm for least-squares estimation of nonlinear parameters," *J. Soc. Ind. Appl. Math.*, vol. 11, no. 2, pp. 431–441, 1963. [Online]. Available: http://www.jstor.org/stable/2098941

[26] T. F. Coleman and Y. Li, "An interior trust region approach for nonlinear minimization subject to bounds," *SIAM J. Optim.*, vol. 6, no. 2, pp. 418–445, 1996.

[27] A. Fettweis, "Parametric representation of Brune functions," *Int. J. Circuit Theory Appl.*, vol. 7, no. 1, pp. 113–119, Jan. 1979, doi: 10.1002/cta.4490070112.

[28] J. Pandel and A. Fettweis, "Broadband matching using parametric representations," in *Proc. IEEE Int. Symp. Circuits Syst.*, vol. 41, pp. 143–149, Jul. 1985.

[29] B. S. Yarman and A. Fettweis, "Computer-aided double matching via parametric representation of Brune functions," *IEEE Trans. Circuits Syst.*, vol. 37, no. 2, pp. 212–222, Feb. 1990, doi: 10.1109/31.45713.

[30] B. S. Yarman, *Design of Ultra Wideband Power Transfer Networks*. Hoboken, NJ, USA: Wiley, 2010.

[31] B. S. Yarman, S. Yarman, A. Aksen, R. Köprü, N. Kumar, Ç. Aydin, and P. Chacko, "Computer aided Darlington synthesis of an all purpose immittance function," *Electrica*, vol. 16, no. 1, pp. 2027–2037, 2016.

[32] B. S. Yarman, A. Aksen, R. Kopru, C. Aydin, and C. Atilla, "Computer aided high precision Darlington synthesis for real frequency matching," in *Proc. IEEE Benjamin Franklin Symp. Microw. Antenna Sub-systems Radar, Telecommun., Biomed. Appl. (BenMAS)*, Sep. 2014, pp. 1–3, doi: 10.1109/BenMAS.2014.7529474.

[33] A. Kilinc and B. S. Yarman, "High precision LC ladder synthesis. Part I: Lowpass ladder synthesis via parametric approach," *IEEE Trans. Circuits Syst. I, Reg. Papers*, vol. 60, no. 8, pp. 2074–2083, Aug. 2013, doi: 10.1109/TCSI.2013.2239163.

[34] B. S. Yarman and A. Kilinc, "High precision LC ladder synthesis. Part II: Immittance synthesis with transmission zeros at DC and infinity," *IEEE Trans. Circuits Syst. I, Reg. Papers*, vol. 60, no. 10, pp. 2719–2729, Oct. 2013, doi: 10.1109/TCSI.2013.2244315.

[35] Z. Dai, S. He, J. Pang, C. Huang, J. Peng, Z. Yang, and M. Li, "Lowpass network synthesis using 'Feldtkeller correction approach,'" *IEEE Access*, vol. 7, pp. 27970–27982, 2019, doi: 10.1109/ACCESS.2019.2894408.

[36] B. S. Yarman, A. Kilinc, and A. Aksen, "Immitance data modelling via linear interpolation techniques: A classical circuit theory approach," *Int. J. Circuit Theory Appl.*, vol. 32, no. 6, pp. 537–563, Nov. 2004, doi: 10.1002/cta.295.
[37] *PathWave Advanced Design System (ADS) From Keysight*. Accessed: Apr. 2022. [Online]. Available: https://www.keysight.com/zz/en/products/software/pathwave-design-software/pathwave-advanced-design-system.html
[38] A. Grebennikov, N. Kumar, and B. S. Yarman, *Broadband RF and Microwave Amplifiers*. Boca Raton, FL, USA: CRC Press, 2015.
[39] A. Aksen and B. S. Yarman, "A semi-analytical procedure to describe lossless two-ports with mixed lumped and distributed elements," in *Proc. IEEE Int. Symp. Circuits Syst. (ISCAS)*, May/Jun. 1994, pp. 205–208, doi: 10.1109/ISCAS.1994.409340.
[40] B. S. Yarman and A. Aksen, "An integrated design tool to construct lossless matching networks with mixed lumped and distributed elements," *IEEE Trans. Circuits Syst. I, Fundam. Theory Appl.*, vol. 39, no. 9, pp. 713–723, Sep. 1992, doi: 10.1109/81.250162.
[41] R. W. Rhea, *HF Filter Design and Computer Simulation*. London, U.K.: Institution of Engineering and Technology, 1994.
[42] *Taconic Corporation*. Accessed: Apr. 2022. [Online]. Available: http://www.taconic.co.kr/english/pages/sub02_03.php
[43] *KYOCERA AVX Corporation*. Accessed: 2022. [Online]. Available: https://www.kyocera-avx.com/
[44] *Coilcraft Corporation*. Accessed: Apr. 2022. [Online]. Available: https://www.coilcraft.com/
[45] *Murata Corporation*. Accessed: Apr. 2022. [Online]. Available: https://www.murata.com/en-eu/products

SEDAT KILINC received the B.Sc. degree from Yildiz Technical University, Istanbul, in 2012, and the M.Sc. degree in electronics and communications engineering from Istanbul Technical University, in 2015. He is currently pursuing the Ph.D. degree with the Technical University of Istanbul. He has been studying as a Research Assistant at Istanbul University-Cerrahpaşa, since 2012. His research interests include design of RF power amplifiers, semi-analytical techniques for wideband microwave power transfer networks, and synthesis with lumped/distributed circuit elements.

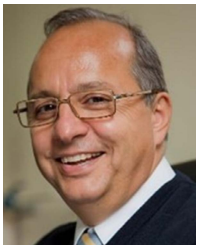

BINBOGA SIDDIK YARMAN (Life Fellow, IEEE) received the B.Sc. degree from the Technical University of Istanbul, in 1974, the M.Sc. degree from the Stevens Institute of Technology, Hoboken, NJ, USA, in 1977, and the Ph.D. degree from Cornell University, Ithaca, NY, USA, in 1982.

He was a member of Technical Staff at the General David Sarnoff Microwave Technology and Research Center (previously RCA Sarnoff Research Center), Princeton, NJ, USA. He has worked as a Professor and an Administrator at various universities, such as Anadolu University, Middle East Technical University, Istanbul University, Isik University, Turkey; Ruhr University, Germany; Tokyo Institute of Technology, Japan; and Wuhan Technology University, China. He is currently with Istanbul University, the Technical University of Istanbul, and Lincoln University, U.K. He is one of the founders of Savronik Group of Companies and recently serves as the Chairman for the Board of Directors of Savronik International Company. He is the Founding Chairman of RFT Research and Technology Corporation. He was the Founding President (1996–2004) and has served as the Chairman for Board of Trustees (2010–2017) of Isik University. He is the inventor/co-inventor of many RF and microwave circuit design methods known as the "real frequency techniques" and speech, image, and video encoding/decoding techniques known as "SYMPES" and the originator of the "Sympes-Phone" or in short "Symphone." He has published more than 300 papers in the field of microwave engineering, circuit and systems, signal processing, mathematical modeling, and decision making. He has published six major research/text books, namely *Design of Ultra Wideband Antenna Matching Networks* (Springer, 2008), *Design of Ultra Wideband Power Transfer Networks* (Wiley, 2010), *Intelligence Based Decision Making* (Nobel Press of Turkey, 2014), *Broadband Microwave and RF Power Amplifiers* (CRC-Taylor & Francis, November 2016), *Design of Broadband RF and Microwave Power Amplifiers* (IET of U.K., 2020), and *Design of Digital Phase Shifters for Multipurpose Communication Systems* (River Publisher, 2020). He holds five U.S. and nine Turkish patents.

Dr. Yarman was selected as a member of the New York Academy of Science in 1998. He is an Alexander Von Humboldt Fellow of Germany and a Salzburg Fellow of USIS (1985). He was a recipient of the Young Turkish Scientist Award of the Republic of Turkey in 1986, the Technology Award of the Scientific and Research Council of Turkey in 1987, and the Research Award of Alexander von Humboldt Foundation of Germany in 1987. He was selected as the "Man of the Year in Science and Technology" by Cambridge Biography Center of U.K. (1998).

SERDAR OZOGUZ was born in Istanbul, Turkey. He received the B.Sc., M.Sc., and Ph.D. degrees in electronics engineering from Istanbul Technical University, in 1991, 1993, and 2000, respectively. Since 2009, he has been working as a Full Professor at Istanbul Technical University. He is currently a Full Professor in electronics and teaching graduate and undergraduate courses. He is the coauthor of 150 articles published in scientific reviews or conference proceedings. His research interests include analog circuit design, chaotic circuits, and chaos applications.